Liquidus temperature measurements for modeling oxide glass systems relevant to nuclear waste vitrification

Jonathan B. Hanni, Eric Pressly, Jarrod V. Crum, Kevin B.C. Minister, Diana Tran, Pavel Hrma, and John D. Vienna[a)]
Environmental Technology Division, Pacific Northwest National Laboratory, Richland, Washington 99354

(Received 9 March 2005; accepted 30 August 2005)

Liquidus temperatures (T_L) were measured, and primary phases were determined for 50 (from an initial test matrix of 76) compositions within the Al_2O_3–B_2O_3–CaO–Na_2O–SiO_2 glass-forming system and its constituent ternary subsystems. Strong linear correlations have been found between composition and T_L for melts within the same primary phase fields. The T_L and primary phase data are being used to develop and refine a modified associate species model (ASM). The impacts of Fe_2O_3, Li_2O, NiO, ZrO_2, Cr_2O_3, ZnO, and MnO additions on the T_L of two baseline glass compositions are reported. These data are intended as benchmarks for further expansion of the ASM or other silicate melt solution models of nuclear waste glasses.

I. INTRODUCTION

The Department of Energy (DOE) is currently constructing the world's largest nuclear waste vitrification facility to treat and immobilize nuclear wastes from the Hanford Site in southeastern Washington State.[1] One of the primary concerns for operation on the electric melter in the vitrification plant is the deleterious effects of crystal accumulation in the melter. Crystals generally have higher density than the glass melt and tend to settle to the bottom of the melter where they can clog pouring spouts[2] or cause electrical short circuits.[3]

Many of the Hanford wastes contain high concentrations of soda and alumina, and nepheline ($NaAlSiO_4$) may precipitate from these glasses as the melt cools. Nepheline formation during cooling may significantly decrease the chemical durability of the glass since each mole of nepheline formed removes two moles of network-forming components (one mol each of Al and Si) for each mol of modifier (Na).[2] Constraints placed on glass composition to limit the formation of crystals in the melter or during cooling often reduce the amount of waste that can be tolerated in the glass.[4,5]

To better formulate nuclear waste glasses, a model capable of predicting the thermodynamics of waste glass melts is needed. With this model, one should be able to calculate the temperature at which crystals can form in multicomponent waste glass melts (the liquidus temperature T_L) as a function of composition. A partnership between Oak Ridge National Laboratory, Pennsylvania State University, and Pacific Northwest National Laboratory (PNNL) has been established to develop thermodynamic models for the waste glass melt solution. A modified associate species model (ASM) is being developed.[6–9] To facilitate the development of the ASM T_L data sets from glass melt systems with progressively more components are being measured.

Waste glasses are primarily composed of Al_2O_3, B_2O_3, Na_2O, CaO, Li_2O, Fe_2O_3, ZrO_2, and SiO_2.[4] Even relatively small concentrations of ZnO, Cr_2O_3, NiO, and MnO strongly impact the amount and composition of the crystalline phases that form in these melts as they cool.[4,7,10–14] Table I summarizes the concentrations of oxides in typical Hanford waste glasses; also shown are the concentrations of oxides in typical wastes that are being vitrified at the Defense Waste Processing Facility (DWPF) at DOE's Savannah River site near Aiken, South Carolina.[15] In this paper, we report the T_L and primary phases for melts made up of subsets of these 12 components. The initial testing focused on the five-component Al_2O_3, B_2O_3, Na_2O, CaO, and SiO_2 (ABCNS) system. Additional compositions were selected from the ternary systems CaO, Na_2O, and SiO_2 and CaO, Al_2O_3, and SiO_2. Two baseline glasses were selected from the ABCNS glasses in this study, and varying concentrations of Fe_2O_3, Li_2O, NiO, ZrO_2, Cr_2O_3, ZnO, and MnO were added individually to determine their effects on the T_L and primary phase formation for the baseline glass melts.

a)Address all correspondence to this author.
e-mail: john.vienna@pnl.gov
DOI: 10.1557/JMR.2005.0424

CAMBRIDGE JOURNALS
http://journals.cambridge.org Downloaded: 28 Mar 2015 IP address: 165.91.74.118

TABLE I. Composition ranges for typical waste glass components (mass%).[15]

	Hanford	LAW	Hanford	HLW	DWPF	HLW
Al_2O_3	2	12	3	18	2.4	5.5
B_2O_3	5	15	4	20	6.8	11.5[a]
CaO	0	8	0	8	0.7	1.3
Cr_2O_3	⋯	⋯	0	1	0	0.2
Fe_2O_3	0	8[a]	1	18	8.5	12.4
K_2O	0	5[a]	0.05	3	2.1	2.6
Li_2O	0	6	0.05	6	4.3	5
MgO	0	4.3	0.05	3	0[a]	2.1
MnO	⋯	⋯	0.02	10	1.1	2.8
Na_2O	5	23	5	20	7.8	15[a]
NiO	⋯	⋯	0.1	3	0.1	1.2
P_2O_5	0	3	0	3	⋯	⋯
SO_3	0	1.5	0	0.5		
SiO_2	36	60	33	60	49.1	55.1
SrO	⋯	⋯	0	10	⋯	⋯
ThO_2	⋯	⋯	0	4	⋯	⋯
TiO_2	0	5	0	2	0.2	0.4
U_3O_8	⋯	⋯	0	12	0.8	5
ZnO	0	3	0	3	⋯	⋯
ZrO_2	0	6	0	10	⋯	⋯

[a]Modified ranges.

II. DESCRIPTION OF MODIFIED ASSOCIATE SPECIES MODEL

The ASM, originally developed by Hastie and Bonnel[16,17] and Shakhmatkin et al.[18,19] has been used successfully to calculate the solution behavior of multicomponent oxide minerals and melts. In the model, the solution is represented as a mixture of associate species such as $NaAlO_2$, $NaBO_2$, and Si_2O_4. The associate species contain between one and three non-oxygen types of elements whose number must add up to 2 to provide a consistent basis for molecular size (e.g., $NaAlSiO_4$ stoichiometry is multiplied by ⅔ or $Na_{0.67}Al_{0.67}Si_{0.67}O_{2.67}$ to maintain appropriate non-oxygen content). In the basic ASM, the species in the liquid are mixed ideally to generate a melt solution. However, in the modified ASM being developed, a limited number of regular solution terms are included to allow for immiscibility in the melt. The excess enthalpy of mixing is taken into account through the energy of formation for the liquid associate species. This model has enjoyed great success in complicated oxide minerals and melts because of its simple construction and implicit tie to the type of bonding that occurs. Various species seldom would have more than two types of elements as second nearest neighbors (second to oxygen) in silicate melts. The components with the strongest mixing interactions are likely to be within the associate species. Therefore, the ideal solution is a good first approximation for mixing energies. Besmann, Spear, and colleagues[6–9] give detailed discussions of the advantages of this model for glass melts and discuss its preliminary development.

III. EXPERIMENTAL METHODS

Liquidus temperature has been measured for seven test matrices, three containing (mol%): Al_2O_3 (0.1–25), B_2O_3 (0–20), CaO (0–20), Na_2O (9.1–33.3), and SiO_2 (35.7–80); one comprised of (mol%): CaO (22–44), Na_2O (2.1–16), and SiO_2 (51–67); one containing (mol%) CaO (34–52), Al_2O_3 (1.7–11), and SiO_2 (43–57); and two others, each composed of a baseline glass chosen from the initial test matrix with individual additions of the following components (mol%): Fe_2O_3 (0–5), Li_2O (0–13), NiO (0–2), ZrO_2 (0–3), Cr_2O_3 (0–0.25), ZnO (0–4.5), and MnO (0–5).

A. Al_2O_3–B_2O_3–CaO–Na_2O–SiO_2 glass network

The ABCNS test matrices are presented in Table II. These compositions are all based primarily on the Na_2O–Al_2O_3–SiO_2 ternary system (see Fig. 1).[20] Glasses ABCNS-01 through -04 were chosen because they are stoichiometrically equivalent to $NaAlSiO_4$ (nepheline), $NaAlSi_2O_6$, $NaAlSi_3O_8$ (albite), and $NaAlSi_4O_{10}$, respectively, although glass -04 lies within an immiscibility dome. These four compounds are well suited for comparison with both measured T_L data and ASM-predicted T_L because they are well documented in the literature.[20] Glasses ABCNS-05 through -08 are based upon the first four with the addition of B_2O_3 in a 1:1:1 ratio to Na_2O and Al_2O_3; likewise, glasses ABCNS-09 through -12 have CaO in a 1:1:1 ratio to Na_2O and Al_2O_3, and -13 through -16 contain B_2O_3 and CaO, both in 0.5:1:1 ratios to Na_2O and Al_2O_3. Glasses ABCNS-17 through -40 are statistically formulated to cover a broad range of compositions for all five components in a three compositional layer design (outer layer, inner layer, and centroid). Glass ABCNS-17 is the compositional centroid of these glass formulations, ABCNS-18 through -27 comprise an outer layer, and ABCNS-27 through -40 are the inner layer.

Liquidus temperatures could not be measured for many of the glasses within the initial test matrix because of liquid–liquid immiscibility, inability to fabricate glass melts at ⩽1600 °C, or measurement difficulties; T_L was too high for the furnaces (maximum temperature ~1600 °C) or too low to be measured in laboratory time scales (e.g., equilibration time of months or years rather than days). Glasses ABCNS-41 through -48 were added to the matrix to provide additional data points. The ABCNS-2-XX glasses were also added to the matrix to generate additional Al_2O_3–B_2O_3–Na_2O–SiO_2 T_L data. Glass ABCNS-05 was re-measured with an alternate technique (melt-back, see Sec. III. E) and labeled ABCNS-05B. Melt-back was used to measure T_L for the ABCNS-2-XX glasses as well.

The ABCNS-3-XX glasses were added to measure the effects of B_2O_3 concentration near the boundaries of the

CAMBRIDGE JOURNALS
http://journals.cambridge.org Downloaded: 28 Mar 2015 IP address: 165.91.74.118

TABLE II. Al_2O_3–B_2O_3–CaO–Na_2O–SiO_2 (ABCNS) glass test matrix. Compositions are given in mol fraction. T_L values have a measurement uncertainty of ±5 °C.

Glass ID	Al_2O_3	B_2O_3	CaO	Na_2O	SiO_2	T_L (°C)	Primary phase
ABCNS-01	0.2500	0.0000	0.0000	0.2500	0.5000	1510	Carnegieite
ABCNS-02	0.1667	0.0000	0.0000	0.1667	0.6667	1124	Nepheline
ABCNS-03	0.1250	0.0000	0.0000	0.1250	0.7500	1085	Below XRD detection limit
ABCNS-04	0.1000	0.0000	0.0000	0.1000	0.8000	…	…
ABCNS-05	0.2000	0.2000	0.0000	0.2000	0.4000	875	Nepheline
ABCNS-05B	0.2000	0.2000	0.0000	0.2000	0.4000	875	Nepheline
ABCNS-06	0.1429	0.1429	0.0000	0.1429	0.5714	…	…
ABCNS-07	0.1111	0.1111	0.0000	0.1111	0.6667	…	…
ABCNS-08	0.0909	0.0909	0.0000	0.0909	0.7273	…	…
ABCNS-09	0.2000	0.0000	0.2000	0.2000	0.4000	1303	$Na_{1.45}Al_{1.45}Si_{0.55}O_4$, gehlenite
ABCNS-10	0.1429	0.0000	0.1429	0.1429	0.5714	1133	Nepheline
ABCNS-11	0.1111	0.0000	0.1111	0.1111	0.6667	1190	Pseudowollastonite
ABCNS-12	0.0909	0.0000	0.0909	0.0909	0.7273	…	…
ABCNS-13	0.2000	0.1000	0.1000	0.2000	0.4000	1147	Nepheline
ABCNS-14	0.1429	0.0714	0.0714	0.1429	0.5714	955	Andesine
ABCNS-15	0.1111	0.0556	0.0556	0.1111	0.6667	1100	Andesine
ABCNS-16	0.0909	0.0455	0.0455	0.0909	0.7273	…	…
ABCNS-17	0.1196	0.0718	0.0771	0.1506	0.5809	1001	Wollastonite
ABCNS-18	0.0909	0.1176	0.1240	0.1068	0.5607	1001	Wollastonite
ABCNS-19	0.1712	0.0200	0.1516	0.2225	0.4347	1198	Carnegieite
ABCNS-20	0.1901	0.0000	0.0534	0.1753	0.5812	…	…
ABCNS-21	0.0909	0.0914	0.0271	0.0909	0.6996	…	…
ABCNS-22	0.1166	0.1166	0.1308	0.1946	0.4414	935	Nepheline
ABCNS-23	0.0909	0.0000	0.0171	0.1878	0.7042	…	…
ABCNS-24	0.2044	0.0047	0.0713	0.0987	0.6209	…	…
ABCNS-25	0.0909	0.1070	0.0219	0.0909	0.6893	…	…
ABCNS-26	0.1867	0.0000	0.0285	0.1350	0.6498	…	…
ABCNS-27	0.0909	0.1030	0.1086	0.1663	0.5311	984	Wollastonite
ABCNS-28	0.1274	0.0622	0.0500	0.1375	0.6229	…	…
ABCNS-29	0.0764	0.1156	0.0915	0.1375	0.5790	…	…
ABCNS-30	0.1014	0.1005	0.0912	0.1375	0.5694	984	Wollastonite
ABCNS-31	0.0953	0.0782	0.1045	0.2105	0.5115	935	Wollastonite
ABCNS-32	0.1037	0.0542	0.0921	0.1394	0.6105	1061	Wollastonite
ABCNS-33	0.1442	0.0500	0.0740	0.1727	0.5591	1001	Nepheline/wollastonite
ABCNS-34	0.1594	0.0830	0.0661	0.1435	0.5480	1052	Anorthite/albite
ABCNS-35	0.0883	0.0819	0.0792	0.1927	0.5578	915	Wollastonite
ABCNS-36	0.1126	0.0987	0.0982	0.1563	0.5342	984	Nepheline
ABCNS-37	0.1431	0.1021	0.0746	0.1491	0.5312	905	Anorthite/albite
ABCNS-38	0.0639	0.1275	0.1035	0.1892	0.5158	886	Wollastonite
ABCNS-39	0.1367	0.0644	0.0753	0.1804	0.5432	974	Nepheline
ABCNS-40	0.1125	0.1156	0.0911	0.1484	0.5324	956	Wollastonite
ABCNS-41	0.1429	0.0807	0.0889	0.2119	0.4757	1044	Nepheline
ABCNS-42	0.2418	0.2000	0.0000	0.1582	0.4000	…	Corundum
ABCNS-43	0.0142	0.0383	0.0830	0.2054	0.6591	841	$Na_2Ca_3Si_6O_{16}$
ABCNS-44	0.1653	0.0895	0.0953	0.1005	0.5494	1198	Anorthite/albite
ABCNS-45	0.0455	0.0460	0.0587	0.2315	0.6183	814	Combeite
ABCNS-46	0.2331	0.1424	0.0000	0.1999	0.4246	…	Corundum
ABCNS-47	0.0006	0.1272	0.0067	0.1312	0.7343	1080	Cristobalite/tridymite
ABCNS-48	0.1486	0.0735	0.0988	0.1000	0.5792	1167	Anorthite/albite
ABCNS-2-01	0.2222	0.1111	0.0000	0.2222	0.4444	1178	Nepheline
ABCNS-2-02	0.1538	0.0769	0.0000	0.1538	0.6154	…	…
ABCNS-2-03	0.1176	0.0588	0.0000	0.1176	0.7059	…	…
ABCNS-2-04	0.0952	0.0476	0.0000	0.0952	0.7619	…	…
ABCNS-3-01	0.1234	0.0502	0.0000	0.3498	0.4766	990	Nepheline
ABCNS-3-01b	0.1234	0.0502	0.0000	0.3498	0.4766	990	Nepheline
ABCNS-3-02	0.1740	0.0515	0.0000	0.1275	0.6470	1409	Mullite/corundum
ABCNS-3-03	0.0842	0.0489	0.0000	0.3485	0.5184	830	Nepheline
ABCNS-3-04	0.1920	0.0521	0.0000	0.1375	0.6184	1347	Mullite/corundum
ABCNS-3-05	0.1079	0.1693	0.0000	0.3059	0.4169	830	Nepheline
ABCNS-3-06	0.0739	0.1656	0.0000	0.3057	0.4548	718	Nepheline

(continued)

CAMBRIDGE JOURNALS
http://journals.cambridge.org Downloaded: 28 Mar 2015 IP address: 165.91.74.118

TABLE II. Al_2O_3–B_2O_3–CaO–Na_2O–SiO_2 (ABCNS) glass test matrix. Compositions are given in mole fraction. T_L values have a measurement uncertainty of ±5 °C. (continued)

Glass ID	Al_2O_3	B_2O_3	CaO	Na_2O	SiO_2	T_L (°C)	Primary phase
ABCNS-3-07	0.1517	0.1731	0.0000	0.1111	0.5641	1290	Mullite/aluminum borate
ABCNS-3-08	0.1671	0.1748	0.0000	0.1197	0.5383	1315	Mullite/aluminum borate
ABCNS-4-01	0.0000	0.0000	0.4442	0.0413	0.5145	…	…
ABCNS-4-02	0.0000	0.0000	0.4072	0.0207	0.5721	…	…
ABCNS-4-03	0.0000	0.0000	0.4055	0.0684	0.526	…	…
ABCNS-4-04	0.0000	0.0000	0.3441	0.0456	0.6103	…	…
ABCNS-4-05	0.0000	0.0000	0.3344	0.1147	0.5509	…	…
ABCNS-4-06	0.0000	0.0000	0.2553	0.0777	0.6671	1298	Pseudowollastonite
ABCNS-4-07	0.0000	0.0000	0.2417	0.1617	0.5966	1193	Pseudowollastonite
ABCNS-4-08	0.0000	0.0000	0.2185	0.122	0.6596	1208	Pseudowollastonite
ABCNS-5-01	0.0413	0.0000	0.4442	0.0000	0.5145	…	…
ABCNS-5-02	0.0207	0.0000	0.4072	0.0000	0.5721	…	…
ABCNS-5-03	0.0684	0.0000	0.4055	0.0000	0.526	…	…
ABCNS-5-04	0.0456	0.0000	0.3441	0.0000	0.6103	1393	Pseudowollastonite
ABCNS-5-05	0.1147	0.0000	0.3344	0.0000	0.5509	1378	Pseudowollastonite
ABCNS-5-06	0.0777	0.0000	0.2553	0.0000	0.6671	1378	Pseudowollastonite
ABCNS-5-07	0.1617	0.0000	0.2417	0.0000	0.5966	1278	Pseudowollastonite
ABCNS-5-08	0.122	0.0000	0.2185	0.0000	0.6596	1288	Pseudowollastonite

nepheline phase field of the Na_2O–Al_2O_3–SiO_2 ternary group. Four base compositions of Na_2O, Al_2O_3, and SiO_2 were measured containing 5 and 15 wt% B_2O_3 (roughly 5 and 15 mol%). Glasses ABCNS-01/-05 and -03/-06 are both on the high sodium end of the nepheline phase field; ABCNS-02/-07 and -04/-08 are in the corundum field on the high alumina side of nepheline. Glass ABCNS-3-01 showed excessive volatility during melting, so a second batch was prepared and melted at a lower temperature (labeled ABCNS-3-01b) to determine whether the volatilization had impacted the composition enough to affect T_L.

B. CaO–Na_2O–SiO_2 and CaO–Al_2O_3–SiO_2 ternary systems

In addition to the ABCNS matrix, which is based primarily on the Na_2O–Al_2O_3–SiO_2 system, two test matrices were developed for measuring T_L for glass compositions within the CaO–Na_2O–SiO_2 and CaO–Al_2O_3–SiO_2 ternary groups.[21,22] The CaO–Na_2O–SiO_2 glasses have been designated ABCNS-4-01 through ABCNS-4-08 and are marked on the ternary phase diagram given in Fig. 2. The CaO–Al_2O_3–SiO_2 glasses are listed as

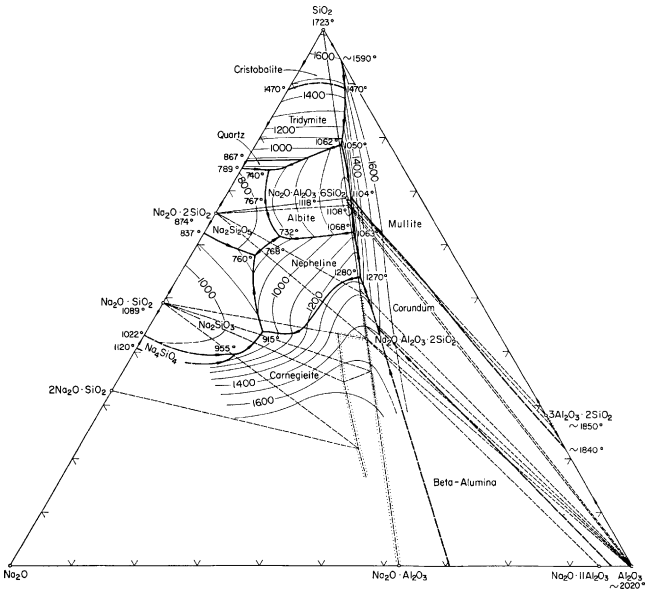

FIG. 1. Phase diagram for the Na_2O–Al_2O_3–SiO_2 ternary oxide system. Reprinted with permission of the American Ceramic Society, www.ceramics.org. Copyright 1964. All rights reserved.[20]

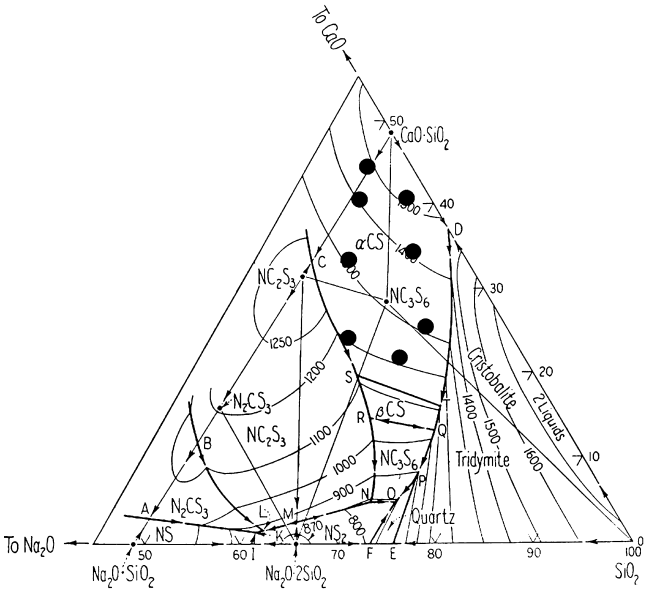

FIG. 2. Phase diagram for the CaO–Na_2O–SiO_2 ternary oxide system. Black circles indicate the compositions of the ABCNS-4-XX glasses. Reprinted with permission of the American Ceramic Society, www.ceramics.org. Copyright 1964. All rights reserved.[20]

CAMBRIDGE JOURNALS
http://journals.cambridge.org Downloaded: 28 Mar 2015 IP address: 165.91.74.118

ABCNS-5-01 through ABCNS-5-08 and marked on the diagram presented in Fig. 3. Compositions for both of these test matrices are also found in Table II.

C. Expanded oxide matrices

Two of the ABCNS glasses were selected as baseline glasses for the expanded oxide matrix. Glass ABCNS-13 was selected because it is stoichiometrically equivalent to nepheline, the most common primary phase in the ABCNS matrix; it is designated ABCNS-6-00 in the new matrix. Glass ABCNS-27, now designated ABCNS-7-00, was chosen because it represents the melts well in the wollastonite ($CaSiO_3$) primary phase field, the second most common phase field in the ABCNS study. The oxides Fe_2O_3, Li_2O, NiO, ZrO_2, Cr_2O_3, NiO, and MnO were added individually to each baseline glass at two or more concentrations by diluting the baseline components in equal relative proportion. Table III presents the ABCNS-6-XX and ABCNS-7-XX test matrices, respectively.

D. Sample fabrication

Glasses were batched at the target compositions listed in Tables II and III with reagent grade chemicals (brand, minimum purity, and particle size information are listed in Table IV); component concentrations were estimated to have <0.05% relative uncertainty (except for Cr_2O_3, which was present in such small quantities that relative uncertainty is estimated to be <0.16%). Each batch was mixed for 5 min in an agate mill and melted for 1 h in Pt/(10%-Rh) crucibles with lids (some with high melting temperatures, such as ABCNS-3-02, were melted for 2 h). A tungsten-carbide mill was used to grind the glasses for 5 min before melting for a second time to ensure homogeneity. Melts were quenched on a stainless steel plate. The quenched glasses were crushed and sieved between #5 and #40 mesh screens to obtain particle sizes between 4 mm and 425 μm. The crushed glass was soaked in ethanol, ultrasonically cleaned for 2 min, and dried overnight at 100 °C to evaporate the ethanol.

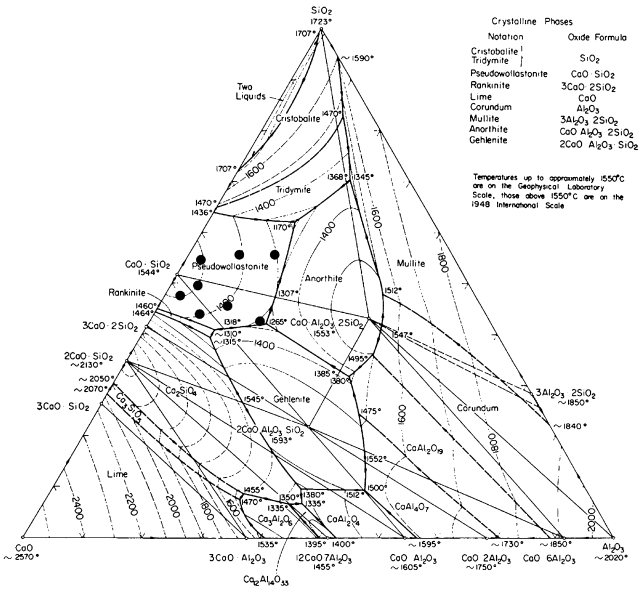

FIG. 3. Phase diagram for the $CaO–Al_2O_3–SiO_2$ ternary oxide system. Black circles indicate the compositions of the ABCNS-5-XX glasses. Reprinted with permission of the American Ceramic Society, www.ceramics.org. Copyright 1964. All rights reserved.[22]

E. T_L measurement

Three measurement techniques were used to determine T_L in this study. For the ABCNS glasses, crushed glasses were placed in Pt/(10%Rh) boats 30 cm long by 0.7 cm wide and 1.4 cm deep. These were placed inside a linear gradient temperature furnace (1 °C/mm) for 24 h, and T_L was determined by locating the point along the long axis of the boat where crystals were undetectable with transmitted light optical microscopy at magnifications of up to 500×.[23] This method worked well to narrow down T_L to an approximate temperature, but isothermal heat treatments were used to bound T_L with much greater precision. Crushed samples were placed in 1 cm^3 Pt/(10%-Rh) crucibles with tight-fitting lids and heat treated at specific temperatures for sufficient time to reach equilibrium (24–96 h). Melt samples were rapidly quenched in air after heat treatment. Optical microscopy was used to determine the presence of crystals in the quenched samples. Measurements continued at different temperatures until T_L was bounded within a 10 °C interval; crystals were present at one temperature and not present at 10 °C higher.

A technique known as melt-back was used to measure T_L for ABCNS-05B and the ABCNS-2-XX glasses. Crushed glass samples were heat treated at temperatures below T_L in 1 cm^3 Pt/Rh crucibles to promote crystallization. The samples were then heat treated at successively higher temperatures until all crystals had dissolved in the melt.

Scanning-electron microscopy with energy dispersive spectroscopy (SEM-EDS) and x-ray diffraction (XRD) were used to identify primary crystalline phases for the glasses. Generally, samples that had been heat treated within 50 °C of T_L were ground into fine powder for XRD analysis; samples that had been heat treated at lower temperatures were used if the higher temperature samples contained insufficient crystalline phase to give a good XRD pattern. SEM was used to determine the presence of crystals that were difficult to see with optical microscopy, to determine the composition of crystals formed, and to confirm the compositions of selected glasses.

CAMBRIDGE JOURNALS
http://journals.cambridge.org Downloaded: 28 Mar 2015 IP address: 165.91.74.118

TABLE III. ABCNS-6-XX and ABCNS-7-XX glass matrices (compositions given in mol percent). Oxide concentrations were added to the ABCNS-6-00 (same composition as ABCNS-13 in Table II) and ABCNS-7-00 (same composition as ABCNS-27 in Table II) baseline glasses.

ABCNS-	Fe_2O_3	Li_2O	NiO	ZrO_2	Cr_2O_3	ZnO	MnO	T_L (°C)	Primary phase
6-00	···	···	···	···	···	···	···	1158	Nepheline
6-01	4.61	···	···	···	···	···	···	1155	Nepheline/hematite
6-02	2.24	···	···	···	···	···	···	1145	Nepheline
6-03	···	12.91	···	···	···	···	···	996	Nepheline
6-04	···	6.70	···	···	···	···	···	1075	Nepheline
6-05	···	···	1.86	···	···	···	···	1155	NiO/nepheline
6-06	···	···	0.93	···	···	···	···	1145	Nepheline
6-07	···	···	···	2.88	···	···	···	1585	Baddeleyite
6-08	···	···	···	1.42	···	···	···	1235	Baddeleyite
6-09	···	···	···	···	0.23	···	···	1245	Nepheline
6-10	···	···	···	···	0.11	···	···	1215	Nepheline
6-11	···	···	···	···	···	4.29	···	1205	Nepheline
6-12	···	···	···	···	···	2.14	···	1155	Nepheline
6-13	···	···	···	···	···	···	4.90	1135	Nepheline
6-14	···	···	···	···	···	···	2.45	1155	Nepheline
6-15	···	···	···	2.15	···	···	···	1485	Baddeleyite
7-00	···	···	···	···	···	···	···	967	Wollastonite
7-01	4.31	···	···	···	···	···	···	940	Wollastonite
7-02	2.09	···	···	···	···	···	···	960	Parawollastonite
7-03	···	12.15	···	···	···	···	···	940	Wollastonite
7-04	···	6.28	···	···	···	···	···	875	Wollastonite
7-05	···	···	1.74	···	···	···	···	960	Parawollastonite
7-06	···	···	0.87	···	···	···	···	1015	Wollastonite
7-07	···	···	···	2.69	···	···	···	995	Parawollastonite
7-08	···	···	···	1.33	···	···	···	985	Wollastonite
7-09	···	···	···	···	0.21	···	···	1125	Nepheline
7-10	···	···	···	···	0.11	···	···	995	Wollastonite
7-11	···	···	···	···	···	4.02	···	1015	Wollastonite
7-12		···	···	···	···	2.00	···	1015	Wollastonite
7-13	···	···	···	···	···	···	4.58	995	Wollastonite
7-14	···	···	···	···	···	···	2.29	1025	Wollastonite
7-15	···	9.27	···	···	···	···	···	885	Wollastonite
7-16	···	3.19	···	···	···	···	···	925	Wollastonite
7-17	···	···	1.30	···	···	···	···	965	Wollastonite
7-18	···	···	0.43	···	···	···	···	1005	Wollastonite

TABLE IV. Desired oxides, chemicals used for batching, chemical brand, minimum chemical purity mass%, and particle size.

Oxide	Chemical	Brand	Purity (%)	Particle size[a]
Al_2O_3	Al_2O_3	Fisher	99	
B_2O_3	H_3BO_3	Noah	99.8	Granular
CaO	$CaCO_3$	Fisher	99	
Na_2O	Na_2CO_3	Fisher	99.5	
SiO_2	SiO_2	Fisher	99	−240 mesh
Fe_2O_3	Fe_2O_3	Fisher	99.999	−199 mesh
Li_2O	Li_2CO_3	Alfa Aesar	99	
NiO	NiO	GFS	99	
ZrO_2	ZrO_2	Noah	99	−325 mesh
Cr_2O_3	Cr_2O_3	Alfa Aesar	98	−325 mesh
ZnO	ZnO	Noah	99.9	−200 mesh
MnO	MnO	Alfa Aesar	99.99	+200 mesh

[a]Some of the chemical manufacturers do not provide specific particle size data. All chemicals used are powders.

IV. T_L AND PRIMARY PHASE MEASUREMENT RESULTS

A. Al_2O_3–B_2O_3–CaO–Na_2O–SiO_2 system

Table II displays T_L and primary phase results for the ABCNS-XX, ABCNS-2-XX, and ABCNS-3-XX glasses. The T_L for glasses ABCNS-04, -08, -12, -16, and -29 were all unable to be measured because of multiple immiscible phases upon fabrication. Liquidus temperature could not be measured for glasses ABCNS-06, -07, ABCNS-2-02, -03, and -04 as the crystallization kinetics were too slow for the techniques used. Glasses ABCNS-20, -21, -23 through -26, and -28 did not completely melt at the highest operating temperature of the furnaces used (~1600 °C). When glasses ABCNS-42 and -46 were melted at 1550 °C and poured, no crystals were present; after a 24-h heat treatment at 1550 °C, both were highly

CAMBRIDGE JOURNALS
http://journals.cambridge.org Downloaded: 28 Mar 2015 IP address: 165.91.74.118

crystalline (crystal fraction greater than 50%). From the XRD patterns, both glasses contained corundum (Al_2O_3), but T_L was higher than the operating temperature of the furnaces. Diffraction peaks consistent with aluminum borate were also found in the XRD pattern from glass ABCNS-42, and shorter heat treatments of 1, 2, and 4 h were performed to determine whether volatilization of sodium borate at 1550 °C could have caused T_L to increase. Loss of Na_2O from glass increases the T_L of melts in most primary phase fields, including corundum. Crystals were found on bubbles and on the surface of the samples from shorter heat treatments, so T_L could not be determined.

B. $CaO–Na_2O–SiO_2$ and $CaO–Al_2O_3–SiO_2$ ternary systems

Table II also contains T_L and primary phase information for the ABCNS-4-XX and ABCNS-5-XX glasses. Glasses ABCNS-4-01 through -05 and ACBNS-5-01 through -03 all crystallized rapidly during quenching from 1500 and 1600 °C; attempts to rapidly quench the melt by placing the crucible in a water bath instead of pouring the melt onto a stainless steel plate were unsuccessful in preventing crystallization. Hence, T_L was not measured for these compositions.

C. $Cr_2O_3–Fe_2O_3–Li_2O–NiO–MnO–ZnO–ZrO_2$ additions

Primary phase and T_L results for the ABCNS-6-XX and ABCNS-7-XX glass matrices are presented in Table III. Figure 4 shows T_L as a function of oxide concentration for each component added to the ABCNS-6-00 and ABCNS-7-00 baseline glasses. Each oxide was added to the baseline glasses at evenly spaced concentrations. The addition of ZrO_2 to the ABCNS-6-00 baseline glass had a profound impact on T_L; it increased by an average of 140 °C per mol% ZrO_2. An additional glass (ABCNS-7-15) was fabricated with 2.15 mol% ZrO_2 to better determine the shape of the increasing T_L curve. Additions of Li_2O and NiO to the ABCNS-7-00 glass yielded both increasing and decreasing T_L values. Two additional glasses with intermediate concentrations of these oxides were fabricated to determine the shape and rate of change of T_L with increasing oxide concentration.

V. DISCUSSION

A. Comparison with literature values

Well-known literature values are available for direct comparison with ABCNS-01 through -04, ABCNS-4-XX, and ABCNS-5-XX glasses (see Figs. 1–3 and Table V). For ABCNS-01 through -03, the T_L data match the literature values reasonably well with a maximum divergence of 33 °C; T_L for ABCNS-04 was indeterminate because of liquid–liquid immiscibility. The observed primary phases for glasses ABCNS-01 and -02 were in agreement with carnegieite and nepheline, as shown in the phase diagram (Fig. 1). The primary phase for ABCNS-03 was undetectable in the XRD patterns after heat treatments 50 °C below T_L.

The ABCNS-4-XX and ABCNS-5-XX glasses were selected such that their compositions all corresponded to T_L isotherms within the pseudowollastonite phase fields of their respective ternary groups. The glasses for which T_L and primary phase could be determined show very strong agreement with the literature values (all of these glasses contain pseudowollastonite, and the largest deviation between T_L values is ~25 °C).

B. Component concentration effects

Empirical modeling of complex oxide melts often requires nonlinear terms. Backman et al.[24] have successfully used polynomial regressive fits; Dreyfus and Dreyfus[25] have used neural networks to model T_L. Empirical models are not the primary goal of this work, but a first-order fit has been used to demonstrate that, when glasses are grouped into their specific primary phase fields, composition effects can be adequately described; these component effects can then be compared to those estimated with the ASM. Regression fits to the nepheline/carnegiete- and wollastonite/pseudowollastonite-phase field glasses include enough data to be statistically significant. An unweighted multiple linear regression of the following form was used

$$T_L = \sum_{i=1}^{N} a_i x_i \quad , \tag{1}$$

where N is the total number of components, and a_i and x_i are the first-order coefficient and mole fraction of the i^{th} component, respectively. This form of first-order model has been used successfully to model T_L for many-component simulated waste glasses within the nepheline phase field.[26]

For the nepheline-phase field glasses, including the 2 from which carnegieite precipitated, a_i values were calculated for all 17 glasses. Glasses ABCNS-3-01 and ABCNS-3-01b were both included in this fit, since both glasses were fabricated and T_L was measured separately. The T_L for ABCNS-05 was measured multiple times with both isothermal and meltback techniques, with both techniques yielding the same value of T_L. Since the same batch was used for all of these measurements, this composition was included only once in the fit. The original ABCNS-XX matrix contained 11 wollastonite-forming ($CaSiO_3$) glasses, including the one pseudowollastonite-phase field glass and the one glass that precipitated both

CAMBRIDGE JOURNALS
http://journals.cambridge.org Downloaded: 28 Mar 2015 IP address: 165.91.74.118

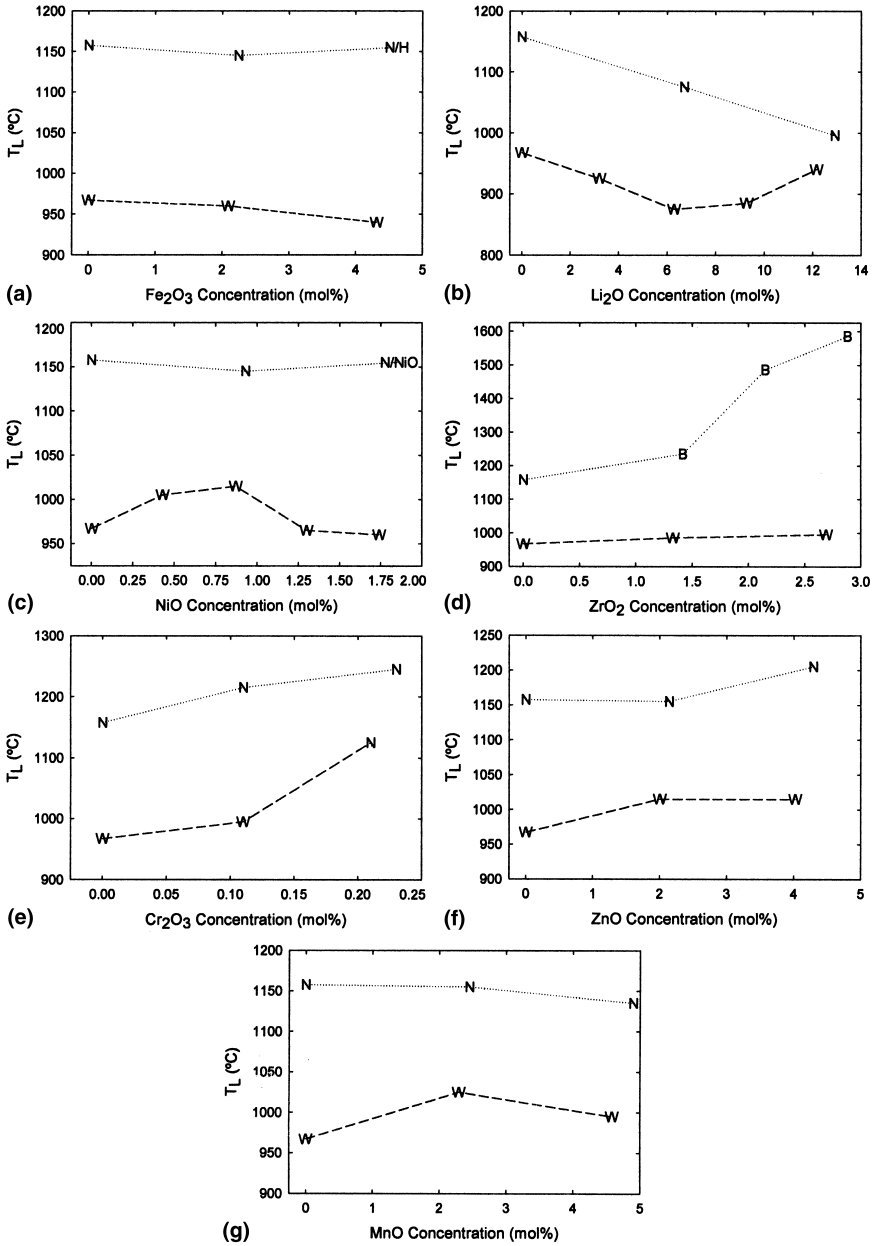

FIG. 4. T_L as a function of mol% of oxide for ABCNS-6-XX (connected with dashed lines) and ABCNS-7-XX glasses (connected with dotted lines). Oxide additions are shown as follows: (a) Fe_2O_3, (b) Li_2O, (c) NiO, (d) ZrO_2, (e) Cr_2O_3, (f) ZnO, and (g) MnO. Phases are given as N = nepheline ($NaAlSiO_4$), W = wollastonite ($CaSiO_3$), B = baddeleyite (ZrO_2), H = hematite (Fe_2O_3), and NiO = nickel oxide (NiO).

nepheline and wollastonite. Equation (1) was used to fit these 11 glasses combined with the eight pseudowollastonite-forming glasses from the ABCNS-4-XX and ABCNS-5-XX matrices. Table VI contains T_L coefficients (a_i values) from both regression calculations.

The linear fits to the data sets from the nepheline- and wollastonite-phase field glasses have large R^2 values; the 17-point linear fit to the nepheline-phase field glasses has an R^2 of 0.924, and R^2 for 19-point wollastonite/pseudowollastonite-phase field glasses is 0.981. These regression results suggest that a very strong first-order correlation exists between T_L and glass composition when compositions are within the same phase field. Furthermore, the phase transition between wollastonite and pseudowollastonite is linear with respect to T_L.

Plots of calculated T_L versus measured T_L are shown in Fig. 5 for the 17-point nepheline model; the 19-point wollastonite model is displayed in Fig. 6. Error bars indicate 95% confidence intervals (U) and have been calculated as follows

$$U = t_{(1-\alpha),n-p} s \sqrt{\mathbf{x}(\mathbf{x}^T\mathbf{X})^{-1}\mathbf{x}^T} \quad , \qquad (2)$$

CAMBRIDGE JOURNALS
http://journals.cambridge.org Downloaded: 28 Mar 2015 IP address: 165.91.74.118

TABLE V. Comparison of ABCNS glasses to literature data (see Figs. 1–3 and associated references).

	Experiment		Literature	
Glass ID	T_L (°C)	Primary phase	T_L (°C)	Primary phase
ABCNS-01	1510 ± 5	Carnegieite	1525[19]	Carnegieite
ABCNS-02	1124 ± 5	Nepheline	1150[19]	Nepheline
ABCNS-03	1085 ± 5	…	1118[19]	Albite
ABCNS-4-06	1298 ± 5	Pseudowollastonite	~1300[20]	Pseudowollastonite
ABCNS-4-07	1193 ± 5	Pseudowollastonite	~1200[20]	Pseudowollastonite
ABCNS-4-08	1208 ± 5	Pseudowollastonite	~1200[20]	Pseudowollastonite
ABCNS-5-04	1393 ± 5	Pseudowollastonite	~1400[21]	Pseudowollastonite
ABCNS-5-05	1378 ± 5	Pseudowollastonite	~1400[21]	Pseudowollastonite
ABCNS-5-06	1378 ± 5	Pseudowollastonite	~1400[21]	Pseudowollastonite
ABCNS-5-07	1278 ± 5	Pseudowollastonite	~1300[21]	Pseudowollastonite
ABCNS-5-08	1288 ± 5	Pseudowollastonite	~1300[21]	Pseudowollastonite

TABLE VI. T_L coefficients a_i [Eq. (1)] for the nepheline and wollastonite linear fits.

Oxide	Nepheline (17 points)	Wollastonite (19 points)
Al_2O_3	3542	723
B_2O_3	−814	−189
CaO	1158	1429
Na_2O	934	147
SiO_2	589	1369

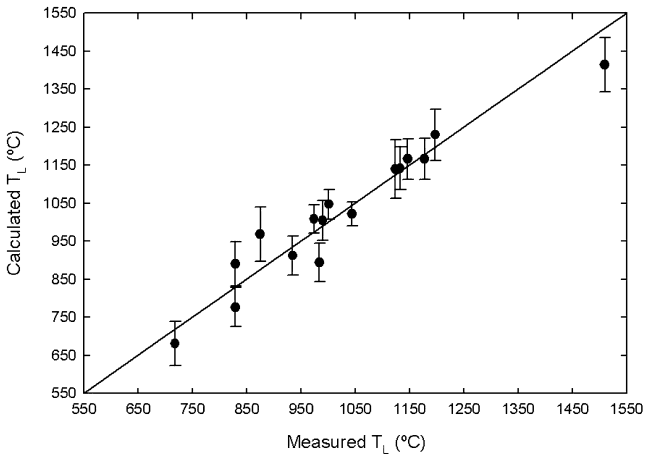

FIG. 5. Comparison of calculated T_L versus measured T_L corresponding to a 17-point fit for glasses that precipitate nepheline (15 glasses) and carnegieite (2 glasses).

where t is the student's t-score corresponding to $1 - \alpha =$ confidence limit, n is the total number of samples, p is the number of predictors (components), s is the standard error, $\mathbf{x}$ is the composition vector for an individual glass, and $\mathbf{X}$ is the composition matrix for all glasses in the model.

C. Expanded oxide matrix data

Overall, the T_L for the ABCNS-7-XX glasses (wollastonite primary phase) changes less after adding the seven

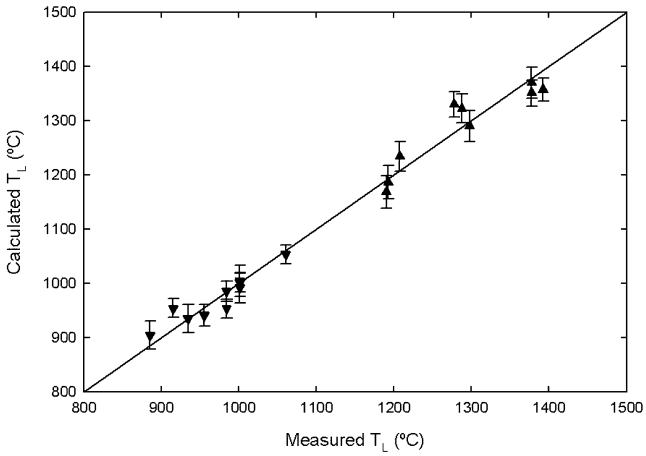

FIG. 6. Comparison of calculated T_L versus measured T_L corresponding to a 19-point fit for glasses that precipitate wollastonite (down-triangles) and pseudowollastonite (up-triangles).

oxides than did the T_L for the ABCNS-6-XX series of glasses (nepheline primary phase). In this baseline glass (ABCNS-7-00), XRD analysis indicated that only the 0.21 mol% Cr_2O_3 addition changed the primary phase from wollastonite to nepheline. The primary phase in the ABCNS-6-00 baseline glass was changed with the addition of the following: ZrO_2, precipitating baddeleyite (ZrO_2) at three ZrO_2 concentrations; Fe_2O_3, precipitating nepheline at all concentrations of Fe_2O_3 and hematite (Fe_2O_3) plus nepheline at 4.61 mol% Fe_2O_3; and NiO, precipitating nepheline at all concentrations and nickel oxide (NiO) plus nepheline at 1.86 mol% NiO.

With the exceptions of Li_2O and ZrO_2, the T_L for the ABCNS-6-XX (nepheline-precipitating) glasses was affected by the additional oxides less than the ABCNS-7-XX glasses. The phase change from nepheline to baddeleyite accounts for the sharp increase in T_L for the ABCNS-6-XX glasses containing ZrO_2. A similar T_L trend is caused by the phase change from wollastonite to nepheline in the ABCNS-7-XX glasses that contain Cr_2O_3. It is not yet clear why such a small concentration

CAMBRIDGE JOURNALS
http://journals.cambridge.org Downloaded: 28 Mar 2015 IP address: 165.91.74.118

of Cr_2O_3 should change the phase field of ABCNS-7-XX from wollastonite to nepheline.

The data ABCNS-7-XX glasses show some intriguing effects of Li_2O or NiO additions on T_L. For NiO, T_L increases sharply with up to 0.43 mol%, levels off until 0.87 mol%, and then decreases sharply to the same value as the baseline glass at 1.3 mol% NiO, followed by a slight decrease when NiO reaches 1.74 mol%. From the XRD patterns, the NiO-bearing ABCNS-7-XX glasses precipitate wollastonite as the primary phase. However, it is possible that an additional phase is present in the sample but was not detected with the XRD technique used.

Crystals in a sample of ABCNS-7-05 that had been heat-treated at 900 °C were analyzed with SEM/EDS to determine if a second phase was present with wollastonite. A SEM micrograph is presented in Fig. 7; the crosshairs in the photo indicate the locations of each EDS spot scan. The mol% of each element and the calculated crystal stoichiometry for crystals A, C, D, and E (see Fig. 7) are given in Table VII. It should be noted that the EDS procedure used is qualitative rather than quantitative.[27] By comparing the ratios of Ca, Ni, and Si, crystals A, D, and E are consistent with $CaSiO_3$ (wollastonite), and crystal C is consistent with $CaNiSi_2O_6$ (niopside[28]).

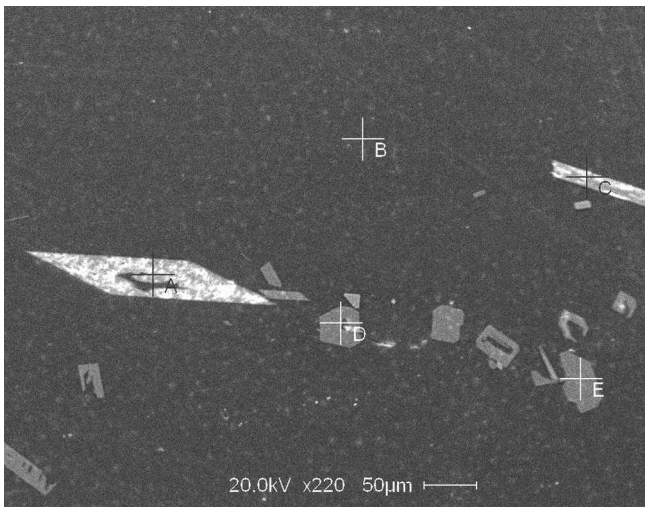

FIG. 7. SEM micrograph of ABCNS-6-05 after heat treatment at 900 °C. Crosshairs indicate locations of EDS spot-scans; these data are given in Table VII.

TABLE VII. EDS results for composition (mol%) and calculated stoichiometries for the crystals found in ABCNS-7-05 (Fig. 7).

Crystal	Ca	Ni	Al	Si	O	Stoichiometry
A	26.03	⋯	0.73	25.41	47.83	$Ca_{1.30}Al_{0.04}Si_{1.27}O_{2.39}$
C	12.32	11.53	1.43	24.2	50.52	$Ca_{1.23}Ni_{1.15}Al_{0.14}Si_{2.42}O_{5.05}$
D	20.01	1.24	2.56	25.32	50.87	$Ca_{1.00}Ni_{0.06}Al_{0.13}Si_{1.27}O_{2.54}$
E	26.5	⋯	⋯	24.51	48.99	$Ca_{1.33}Si_{1.23}O_{2.45}$

Location B in Fig. 7 is the bulk glass, and its composition was analyzed to compare with the target composition of ABCNS-7-05 listed in Table III. To compare the EDS determined and target glass compositions, the EDS results have been renormalized by assuming the glass contains exactly the target concentration of B_2O_3 since boron cannot be measured using the EDS technique used. Table VIII contains the actual and target compositions of ABCNS-7-05.

The ABCNS-7-XX T_L curve for Li_2O appears to have a smoother response than that for NiO. A local minimum occurs at approximately 6.28 mol%, corresponding to a T_L decrease of 90 °C from the T_L of the baseline glass. The ABCNS-6-XX Li_2O curve has a nearly identical 90 °C drop in T_L up to this concentration. The ABCNS-6-XX curve continues to decrease in a nearly linear curve between 6.7 mol% and 12.91 mol%, ending approximately 160 °C lower than the baseline, but the ABCNS-7-XX curve slowly increases 10 °C between 6.28 mol% and 9.27 mol% before sharply climbing 55 °C by 12.15 mol%.

VI. CONCLUSIONS

The primary goal of this work is to provide T_L and primary phase data for a broad range of glass melt compositions to develop and refine the ASM and/or other thermodynamic models for the prediction of waste glass melt phase behavior. To that end, this paper reports the T_L's and primary phases of 51 glass melts in the Al_2O_3–B_2O_3–CaO–Na_2O–SiO_2 system and 35 glass melts each containing one of the following additional components: Cr_2O_3, Fe_2O_3, Li_2O, MnO, NiO, ZnO, and ZrO_2.

The data presented in this paper indicate a close agreement with literature values, where literature values are

TABLE VIII. Target and mean measured (EDS) bulk glass composition of ABCNS-7-05. Ten independent measurements were averaged together to obtain the EDS composition results; uncertainties represent two standard deviations. For the EDS-measured composition, it was assumed that B_2O_3 content in the glass matched that of the target composition.

	B_2O_3 (mol%)	Al_2O_3 (mol%)	CaO (mol%)	Na_2O (mol%)	SiO_2 (mol%)	NiO (mol%)
EDS	⋯	9.13 ± 0.50	11.34 ± 0.92	11.25 ± 2.7	55.89 ± 2.1	2.27 ± 0.30
Target	10.12	8.93	10.68	16.34	52.19	1.74

CAMBRIDGE JOURNALS
http://journals.cambridge.org Downloaded: 28 Mar 2015 IP address: 165.91.74.118

available. This agreement is important as a means of measurement validation. Most of the compositions presented here contain more than three components, so they provide a means of examining how each subsystem of ternary inputs to the ASM or other melt thermodynamic models interact as more components are added; with these data, fit parameters can be adjusted.

Strong linear trends between component concentrations, and T_L values within the nepheline/carnegieite and wollastonite/pseudowollastonite phase fields were found. Similar (linear) trends were found previously in more complex (e.g., 20+ component) waste glass melts from which spinel, nepheline, and zirconia containing phases precipitated.[2,5,10–14]

ACKNOWLEDGMENTS

We would like to thank Dean Moore of PNNL for his help in performing XRD analyses. Mike Schweiger of PNNL contributed his extensive experience with laboratory procedures and measurement techniques to discussions regarding this project. Ted Besmann, Karl Spear, and Nagraj Kulkarni worked diligently to develop and refine the ASM, and they suggested many of the glass compositions studied in this work. Jonathan Hanni, Eric Pressly, and Kevin Minister would like to thank the Office of Fellowship Programs at PNNL for the opportunity to conduct this research project while holding undergraduate and graduate student fellowships at the laboratory. Denis Strachan and Wayne Cosby performed thorough reviews of this document. This work was supported by the U.S. Department of Energy Office of Science through the Environmental Management Science Program grant. Pacific Northwest National Laboratory is operated for the U.S. Department of Energy by Battelle under Contract No. DE-AC05-76RL01830.

REFERENCES

1. *Design Construction, and Commissioning of the Hanford Tank Waste Treatment and Immobilization Plant*. U.S. Department of Energy Contract No. DE-AC27-01RV14136, (2000, as amended).
2. D-S. Kim and P. Hrma: Models for liquidus temperature of nuclear waste glasses. *Ceram. Trans.* **45,** 327 (1994).
3. I.G. Choi, D.F. Bickford, and J.T. Carter: Thermal effects of electrically conductive deposits in a joule-heated melter. *Ceram. Trans.* **29,** 645 (1993).
4. D-S. Kim and J.D. Vienna: Influence of glass property restrictions on Hanford HLW glass volume. *Ceram. Trans.* **132,** 105 (2002).
5. P. Hrma, J.D. Vienna, and M.J. Schweiger: Liquidus temperature limited waste loading maximization for vitrified HLW. *Ceram. Trans.* **72,** 449 (1996).
6. T.M. Besmann and K.E. Spear: Thermochemical modeling of oxide glasses. *J. Am. Ceram. Soc.* **85,** 2887 (2002).
7. T.M. Besmann, K.E. Spear, and J.D. Vienna: Extension of the modified associate species thermochemical model for high-level nuclear waste: Inclusion of chromia, in *Scientific Basis for Nuclear Waste Management XXVI*, edited by R.J. Finch and D.B. Bullen (Mater. Res. Soc. Symp. Proc. **757**, Warrendale, PA, 2003), p. 195.
8. T.M. Besmann, N.S. Kulkarni, and K.E. Spear: Thermochemical and phase equilibria property prediction for oxide glass systems based on the modified associate species approach, in *High Temperature Corrosion and Materials Technology IV,* edited by E. Opila, P. Hou, T. Maruyama, B. Pieraggi, M. McNallan, D. Shifler, and E. Wuchina. (The Electrochemical Society, Pennington, NJ, 2004), p. 557.
9. K.E. Spear, T.M. Besmann, and E.E. Beahm: Thermochemical modeling of glass: Application to high-level nuclear waste glass. *MRS Bull.* **24**(4), 37 (1999).
10. J.V. Crum, P. Hrma, M.J. Schweiger, and G.F. Piepel: Liquidus temperature models for high-level waste glasses that precipitate zirconium-containing crystalline phases. *Ceram. Trans.* **87,** 271 (1998).
11. T. Plaisted, P. Hrma, J. Vienna, and A. Jiricka: Liquidus temperature and primary phase in high-zirconia high-level waste borosilicate glasses, in *Scientific Basis for Nucelar Waste Management XXIII,* edited by R.W. Smith and D.W. Shoesmith (Mater. Res. Soc. Symp. Proc. **608,** Warrendale, PA, 2000), p. 709.
12. J.D. Vienna, P. Hrma, J.V. Crum, and M. Mika: Liquidus temperature-composition model for multi-component glasses in the Fe, Cr, Ni, and Mn spinel primary phase field. *J. Non-Cryst. Solids* **292,** 1 (2001).
13. P. Hrma, J. Vienna, J. Crum, and G. Piepel: Liquidus temperature of high-level waste borosilicate glasses with spinel primary phase, in *Scientific Basis for Nucelar Waste Management XXIII,* edited by R.W. Smith and D.W. Shoesmith (Mater. Res. Soc. Symp. Proc. **608,** Warrendale, PA, 2000), p. 671.
14. M. Mika, M.J. Schweiger, J.D. Vienna, and P. Hrma: Liquidus temperature of spinel precipitating high-level waste glasses, in *Scientific Basis for Nucelar Waste Management XX,* edited by W.J. Gray and I.R. Tridy (Mater. Res. Soc. Symp. Proc., **465,** Pittsburgh, PA, 1997), p. 71.
15. J.D. Vienna: Nuclear waste glasses, in *Properties of Glass-Forming Melts*, edited by L.D. Pye, I. Joseph, and A. Montenero (CRC Press, Boca Raton, FL, 2005). pp. 391–403.
16. J.W. Hastie and D.W. Bonnell: A predictive phase-equilibrium model for multicomponent oxide mixtures. 2. Oxides of Na–K–Ca–Mg–Al–Si. *High Temp. Sci.* **19,** 275 (1985).
17. D.W. Bonnell and J.W. Hastie: A predictive thermodynamic model for complex high-temperature solution phases 11. *High Temp. Sci.* **26,** 313 (1989).
18. B.A. Shakhmatkin, N.M. Vedishcheva, and A.C. Wright: Can thermodynamics relate the properties of melts and glasses to their structure? *J. Non-Cryst. Solids* **293,** 220 (2001).
19. B.A. Shakhmatkin, N.M. Vedishcheva, M.M. Shultz, and A.C. Wright: The thermodynamic properties of oxide glasses and glass-forming liquids and their chemical-structure. *J. Non-Cryst. Solids* **177,** 249 (1994).
20. E.F. Osborn and A. Muan: Fig. 501, in *Phase Diagrams for Ceramists,* Vol. *1*, edited by E.M. Levin, C.R. Robbins, and H.F. McMurdie, (The American Ceramic Society, Columbus, OH, 1964), p. 181.
21. G.W. Morey and N.L. Bowen: *J. Soc. Glass Technol.,* **9**, p. 232 (1925), reprinted as Fig. 482 in *Phase Diagrams for Ceramists,* Vol. 1, edited by E.M. Levin, C.R. Robbins, and H.F. McMurdie (The American Ceramic Society, Columbus, OH, 1964), p. 175.
22. E.F. Osborn and A. Muan: Fig. 630, in *Phase Diagrams for Ceramists,* Vol. 1, edited by E.M. Levin, C.R. Robbins, and H.F. McMurdie (The American Ceramic Society, Columbus, OH, 1964), p. 219.
23. ASTM C829-81: Standard practices for measurement of liquidus temperature of glass by the gradient furnace method. (re-approved

CAMBRIDGE JOURNALS
http://journals.cambridge.org Downloaded: 28 Mar 2015 IP address: 165.91.74.118

1995), in *1999 Annual Book of ASTM Standards,* Vol. 15.02 (American Society for Testing and Materials, West Conshohocken, PA, 1999).
24. R. Backman, K.H. Karlsson, M. Cable, and N.P. Pennington: Model for liquidus temperature of multi-component silicate glasses. *Phys. Chem. Glasses* **38,** 103 (1997).
25. C. Dreyfus and G. Dreyfus: A machine learning approach to the estimation of the liquidus temperature of glass-forming oxide blends. *J. Non-Cryst. Solids* **318,** 63 (2003).
26. H. Li, B. Jones, P. Hrma, and J.D. Vienna: Compositional effects on liquidus temperature of Hanford simulated high-level waste glasses precipitating nepheline ($NaAlSiO_4$). *Ceram. Trans.* **87,** 279 (1998).
27. ASTM E1508-98: Standard guide for quantitative analysis by energy-dispersive spectroscopy, in *2003 Annual Book of ASTM Standards,* Vol. 03.01 (American Society for Testing and Materials, West Conshohocken, PA, 2003).
28. E.B. Pretorius and A. Muan: Stability of $CaNiSi_2O_6$ ("niopside") and activity-composition relations of $CaMgSi_2O_6$ solid solutions at 1350°C. *J. Am. Ceram. Soc.* **75,** 1458 (1992).

CAMBRIDGE JOURNALS
http://journals.cambridge.org Downloaded: 28 Mar 2015 IP address: 165.91.74.118